System Reliability of Floor Diaphragms Framed from Cold-Formed Steel with Wood Sheathing

Aritra Chatterjee, S.M.ASCE[1]; Sanjay R. Arwade, M.ASCE[2]; Benjamin W. Schafer, M.ASCE[3]; and Cristopher D. Moen, M.ASCE[4]

Abstract: A high-fidelity simulation-based system reliability calculation methodology was implemented for steel floor diaphragms framed from cold-formed steel joists topped with wood sheathing, leading to design recommendations that consider the sensitivity of the system performance to fastener component reliability and load paths provided by the sheathing and steel. Diaphragm structural response under in-plane equivalent lateral seismic forces was obtained from high-fidelity computational simulations verified with a full-scale diaphragm test. The model included sheathing-to-joist and joist-to-ledger connection load-slip nonlinearities and randomness from the bearing, tilting, and screw shear, obtained from independent and isolated fastener tests. An uncertainty-modeling scheme provided a statistical distribution for the diaphragm system capacity, which was used to calculate the diaphragm system reliability. The variation in diaphragm system reliability with the fastener component reliability, i.e., the reliability sensitivity, was quantified to guide the diaphragm design to a predefined system-reliability target. **DOI: 10.1061/(ASCE)ST.1943-541X.0001958.**

Author keywords: Diaphragms; Connections; Cold-formed steel; Seismic; System reliability; Resistance factors; Load and resistance factor design (LRFD); Structural safety and reliability.

Introduction

Floor diaphragms play the important role of collecting wind and seismic forces applied to a building and delivering them to the lateral system (Sabelli et al. 2011). In cold-formed steel (CFS) framed low-rise and mid-rise buildings, a sheathed diaphragm is typically constructed over a steel joist floor system (Fig. 1) with wood sheathing connected to the joists with discrete screw fasteners and the joists framing into ledger tracks that are hung from the walls and serve as the chord and/or collector. Multiple load paths are provided by the many structural components and their connections, working as a system, with the benefits of reliability and economy that are well known to engineers and that are difficult to quantify.

For repetitively framed building construction, the structural system reliability is typically higher than a single component's reliability, in both wood (Rosowsky and Ellingwood 1991) and steel (Zhang et al. 2014; Smith et al. 2016) framing. Beneficial system effects exist, theoretically, for redundant systems such as multiple ductile or brittle bars with load sharing (Hendawi and Frangopol 1994), and they have been quantified in practice-oriented studies, such as the case of the reliability advantage of a multiple-girder bridge system over a two-girder bridge system (Ghosn and Moses 1998). The challenge is to quantify these beneficial system effects and to present them for use in the engineering codes and standards that employ a format consistent with component reliability, such as the load and resistance factor design of AISI S100-12 (Ellingwood and Galambos 1982; Galambos 1990; AISI 2012a, b).

The research presented here builds on existing reliability knowledge to define a structural system design process. The approach is applied to a CFS-framed floor diaphragm with wood sheathing considering the realistic sheathing, joist, and fastener-demand probability distributions and the diaphragm system capacity statistics including inelasticity and load sharing. The studied diaphragm system is introduced in the next section, followed by an explanation of the high-fidelity computational simulations that were used to enumerate the force flow, load paths, and redundancy in the diaphragm. The framework was applied to modify a traditional deterministic design in a systematic way to achieve a target system reliability that is not met by the classical design, by using the correlation of the system effects to sheathing fastener performance, i.e., the reliability sensitivity.

CFS Framed Wood-Sheathed Floor Diaphragm System Behavior

Existing experimental research on wood-sheathed diaphragms has confirmed that the fastener connections to the sheathing shear elements dominate the system response. The diaphragm stiffness and strength degrade as the fasteners deform and fracture in shear, and the diaphragm failure can be brittle if the screw edge distances are small enough to allow tearing through the sheathing (NAHBRC 1999). If the panel seams are unblocked, i.e., not connected to the supporting joists with fasteners, the wood sheathing panels slide along each other, shifting more of the in-plane forces into the underlying framing (Countryman 1954; Stillinger 1955; Chatterjee 2016). The fastener connection response is highly variable because of the wood-bearing properties and the variations in fastener

[1]Graduate Research Assistant, Dept. of Civil and Environmental Engineering, Virginia Polytechnic and State Univ., 200 Patton Hall, Blacksburg, VA 24061 (corresponding author). ORCID: https://orcid.org/0000-0001-8323-7131. E-mail: aritrac1@vt.edu

[2]Professor, Dept. of Civil and Environmental Engineering, Univ. of Massachusetts, Amherst, MA 01003. E-mail: arwade@umass.edu

[3]Professor, Dept. of Civil Engineering, Johns Hopkins Univ., 208 Latrobe Hall, Baltimore, MD 21218. E-mail: schafer@jhu.edu

[4]Associate Professor, Dept. of Civil and Environmental Engineering, Virginia Tech, 200 Patton Hall, Blacksburg, VA 24061. E-mail: cmoen@vt.edu

Note. This manuscript was submitted on December 30, 2016; approved on August 3, 2017; published online on December 8, 2017. Discussion period open until May 8, 2018; separate discussions must be submitted for individual papers. This paper is part of the ***Journal of Structural Engineering***, © ASCE, ISSN 0733-9445.

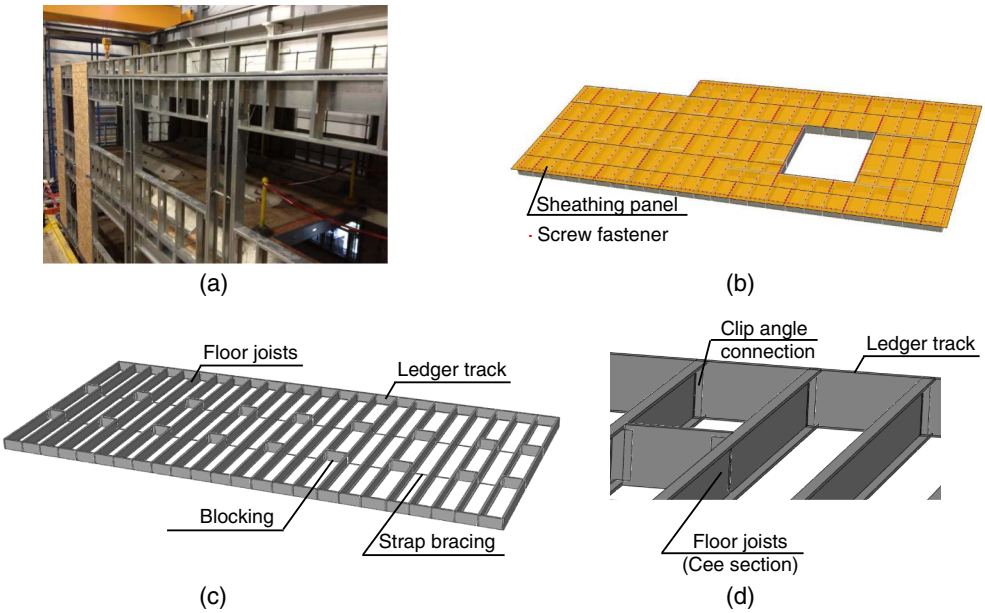

Fig. 1. Cold-formed steel (CFS) framed building is a complex structural system of components and connections: (a) low-rise building showing gravity walls, shear walls, and floor diaphragm under construction (data from Peterman et al. 2016a, © ASCE); (b) typical floor diaphragm system with oriented-strand board (OSB) sheathing connected to steel joist top flanges and ledger tracks with self-drilling screw fasteners (openings used for stairways); (c) cold-formed steel floor framing system showing joists, ledger track, blocking, and strap bracing; (d) floor joist to ledger track connection detail (data from Madsen et al. 2011)

installation (Tao et al. 2016; Peterman et al. 2016b). However, the current diaphragm capacity prediction procedures are highly simplified and define the diaphragm capacity as the sum of the individual fastener strengths at the diaphragm–lateral system interface (LGSEA 1998; AISI 2007a). The design procedure is based on the individual fastener components instead of the full diaphragm system, with several empirical assumptions guiding the component-based design guidelines and little or no formal reliability analyses (ANSI/NFoPA 1991; LGSEA 1998).

Diaphragm Design, Structural Details, and Geometry

The prototype floor diaphragm in this system reliability study was consistent with a ledger-framed cold-formed steel building, i.e., a building where the wall studs frame into ledger tracks at each story level, with sheathing boards sandwiched in between, as shown in Fig. 2. Structural details for other types of cold-formed steel-framed buildings (e.g., balloon framing and precast concrete hollow-core floor diaphragms) can be substantially different and were not considered.

The structural design standards (AISI 2015a) permit the use of two grades of panel material: the higher-quality Structural-1 and the lower-grade "C-D, C-C and other graded wood structural panels," as described in APA (2011). The prototype diaphragm uses C-D, C-C–grade structural oriented-strand boards (OSB), each with the dimensions 1,200 × 2,400 × 18 mm thick with tongue-and-groove edges (Chatterjee et al. 2014), arranged in a staggered configuration and fastened to the supporting cold-formed steel joists (shown in the Fig. 2 plan view). This diaphragm type was recently tested in full-scale building shake-table tests (a CFS-NEES building) considering the 1994 Northridge, California, earthquake ground motions recorded at the Canoga Park and Rinaldi stations (Peterman et al. 2016a).

The sheathing panel type and thickness were chosen on the basis of the joist spacing and the required diaphragm capacity for the anticipated seismic loads, assuming the worst case of flexible and rigid diaphragms (Madsen et al. 2011; AISI 2015a), even though the CFS wood-sheathed diaphragms are permitted to be designed to be flexible, i.e., with a maximum deflection greater than twice the average lateral drift of the shear walls in an earthquake (ASCE 2010). The diaphragm was designed for a load of 37.2 kN (Madsen et al. 2011), which is the controlling ASCE 7-10 diaphragm design load $0.2S_{DS}Iw_{px}$, where $w_{px} = 200$ kN is the seismic weight tributary to the building's second floor (ASCE 2010). The design spectral response acceleration parameter in the short-period range, $S_{DS} = 0.93$, is determined for a design basis earthquake (DBE, 10% probability of occurrence in 50 years), assuming the building is located in Orange County, California.

In the diaphragm, the wood sheathing was connected to the underlying cold-formed steel joists with #10 hex head steel self-tapping and self-drilling screw fasteners (4.7-mm diameter). The fasteners were spaced at 152 mm around the diaphragm perimeter, penetrating the wood panel and the rim tracks. The fastener spacing, 152 mm at the diaphragm edges and 305 mm in the field of the diaphragm where the joists supported the sheathing, was selected on the basis of the AISI S213-07 North American Standard for Cold-Formed Steel Framing—Lateral Design (AISI 2007b), now superseded by AISI S400-15 North American Standard for Seismic Design of Cold-Formed Steel Structural Systems (AISI 2015a). The cold-formed steel joists were 1200S250-97 (SFIA 2015) lipped Cee sections, where the 1200 stands for a 305-mm (12-in.) out-to-out web depth, the 250 stands for a 63.5-mm (2.50-in.) out-to-out flange width, and the 97 corresponds to a minimum base metal thickness of 2.46 mm (0.097 in.).

The joist web was through-fastened to a 1200T200-97 rim track (i.e., an unlipped Cee section) with clip angles that were 38 × 38 mm (1.5 × 1.5 in.) and 279 mm (11 in.) deep, and had a 54 mil or 1.37-mm (0.054-in.) minimum base metal thickness.

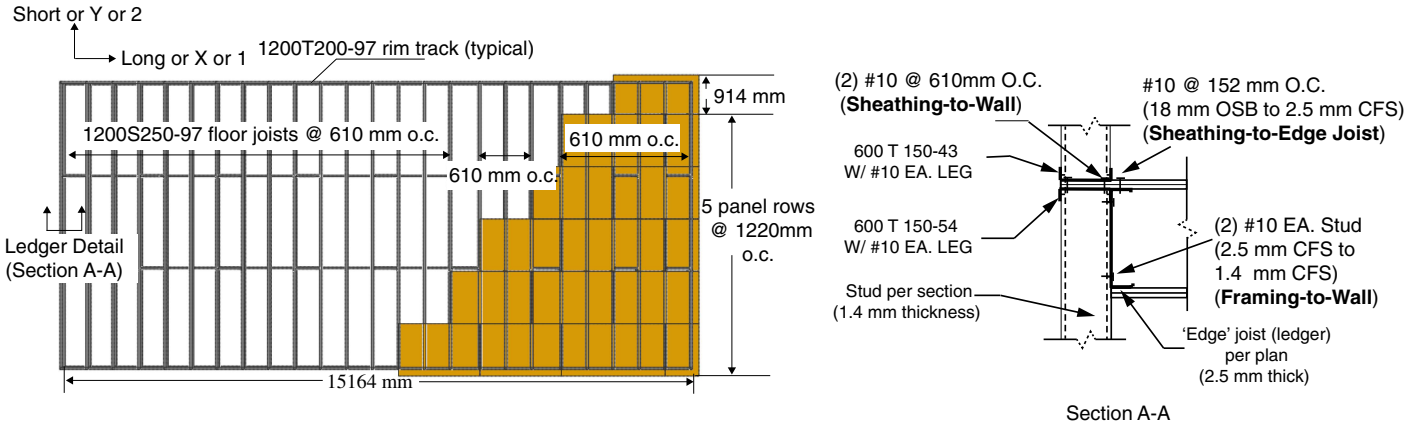

Fig. 2. Wood-sheathed floor diaphragm layout showing cold-formed steel joists, rim tracks, and staggered oriented strand board (OSB) panels; Section A-A shows the ledger framing detail where the floor frames into the short-direction shear walls and the sheathing is sandwiched within the wall (data from Madsen et al. 2011)

Alternate sets of joists were attached to the 1200S162-54 blocking (with a 1.37-mm base metal thickness) with 38 × 102 mm (1.5 × 4 in.), 254 mm (10 in.) deep, 1.37-mm-thick clip angles at approximately one-third and two-thirds of their lengths. The joist and blocking bottom flanges were screw-fastened to 38-mm-wide continuous straps of 1.37-mm thickness. The nominal joist and track yield stress and ultimate stress were 345 and 450 MPa, respectively (Madsen et al. 2011).

The ledger framing detail shown in Fig. 2 is a primary load path for the inertial forces from the diaphragm to the lateral system (e.g., the shear walls). The critical fastener groups, shown in bold in Fig. 2, Section A-A, include the #10 screws connecting the wall track to the sheathing and the wall studs to the edge joists. The edge and field fastener stiffness and strength variability was needed to predict the realized load paths and to calculate the diaphragm system reliability; this information is provided in the next section.

Screw-Fastened Connection Single Shear Load-Deformation Response

Variability in the diaphragm system response derives primarily from the sheathing-to-steel screw through-fastened connections (Florig et al. 2016); these connections are included in these system simulation and design studies. The connection force-deformation behavior was approximated as a multilinear spring on the basis of the recommendations provided in Ibarra et al. (2005) and Moen et al. (2016). The load-deformation model had an initial elastic branch, followed by strain hardening, softening, and failing branches. The multilinear model parameters included the peak (cap) strength F_c; the cap deformation δ_c; the yield strength and deformation F_y and δ_y, respectively; the failure load F_r; the deformation at failure δ_r; and the initial, hardening, softening, and residual stiffness K_e, K_s, K_c, and K_r, respectively (Fig. 3).

To quantify the fastener response variability, fastener tests in single shear were performed with configurations consistent with the typical sheathing-to-joist connectivity; see Chatterjee (2016) for details. Only the detail that matched the sheathing-to-joist and sheathing-to-ledger screw-fastened connections (18-mm OSB to 2.46 mm-steel with #10 fasteners) was characterized experimentally. The sheathing-to-wall fasteners had material properties similar to those of the sheathing-to-framing fasteners (#10 fastener, 1200S250-97 joist and 18-mm-thick OSB) except that they had two shear resisting planes. Therefore it was assumed that the sheathing-to-wall fastener models had the same shape with twice

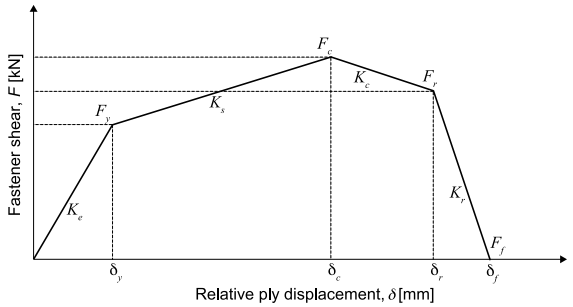

Fig. 3. Screw-fastened connection load-relative ply slip model nomenclature

the stiffness in each leg as sheathing-to-framing fastener models (Fig. 8). The framing-to-wall fastener models (#10 fastener, 2.5-mm steel to 1.4-mm steel) were obtained from the recommendations provided in Tao et al. (2016) using the general expressions for the connection force and stiffness based on the ply thickness, the bearing strength, the fastener diameter, and the manufacturer-reported fastener shear strength. Table 1 presents a summary of the fastener load-deformation parameters and statistics used in the following system-reliability studies.

CFS-Framed Wood-Sheathed Floor Diaphragm Simulations

A high-fidelity (largely shell) finite-element modeling approach is introduced and verified in this section for the wood-sheathed cold-formed steel floor diaphragm shown in Fig. 2. The monotonic diaphragm behavior under the equivalent lateral seismic forces was simulated into the post-peak regime with *ABAQUS*. The model was used to study the load paths and to quantify the diaphragm system capacity and system reliability.

Diaphragm Model Geometry and Material Properties

The cold-formed steel joists, rim tracks, OSB panels, clip angles, strap bracing, and blocking in the floor diaphragm were all modeled with 4 node S4R thin shell elements (Fig. 4). The element aspect ratios were approximately 1:1, and the mesh density was defined in the joists by the flange and web dimensions (Schafer et al. 2010). The steel elastic modulus was assumed as 200 GPa

Table 1. Fastener Load-Deformation Model Parameters for Diaphragm Fastener Connections with Mean μ and Coefficient of Variation (COV)

	F_y		F_c		F_r		F_f		K_e		K_s		K_c		K_r	
Load path	μ (kN)	COV	μ (kN)	COV	μ (kN)	COV	μ (kN)	COV	μ (kN/mm)	COV	μ (kN/mm)	COV	μ (kN/mm)	COV	μ (kN/mm)	COV
Sheathing-to-wall	4.0	0.29	7.8	0.17	7.2	0.14	0	—	7.6	0.30	0.49	0.29	−0.92	1.7	$-\infty$	—
Sheathing-to-edge joist	2.0	0.29	3.9	0.17	3.6	0.14	0	—	3.8	0.33	0.24	0.29	−0.46	1.7	$-\infty$	—
Framing-to-wall	6.1	0.22	8.2	0.03	6.2	0.05	0	—	23	0.23	1.1	0.32	−2.4	0.26	−12	0.50

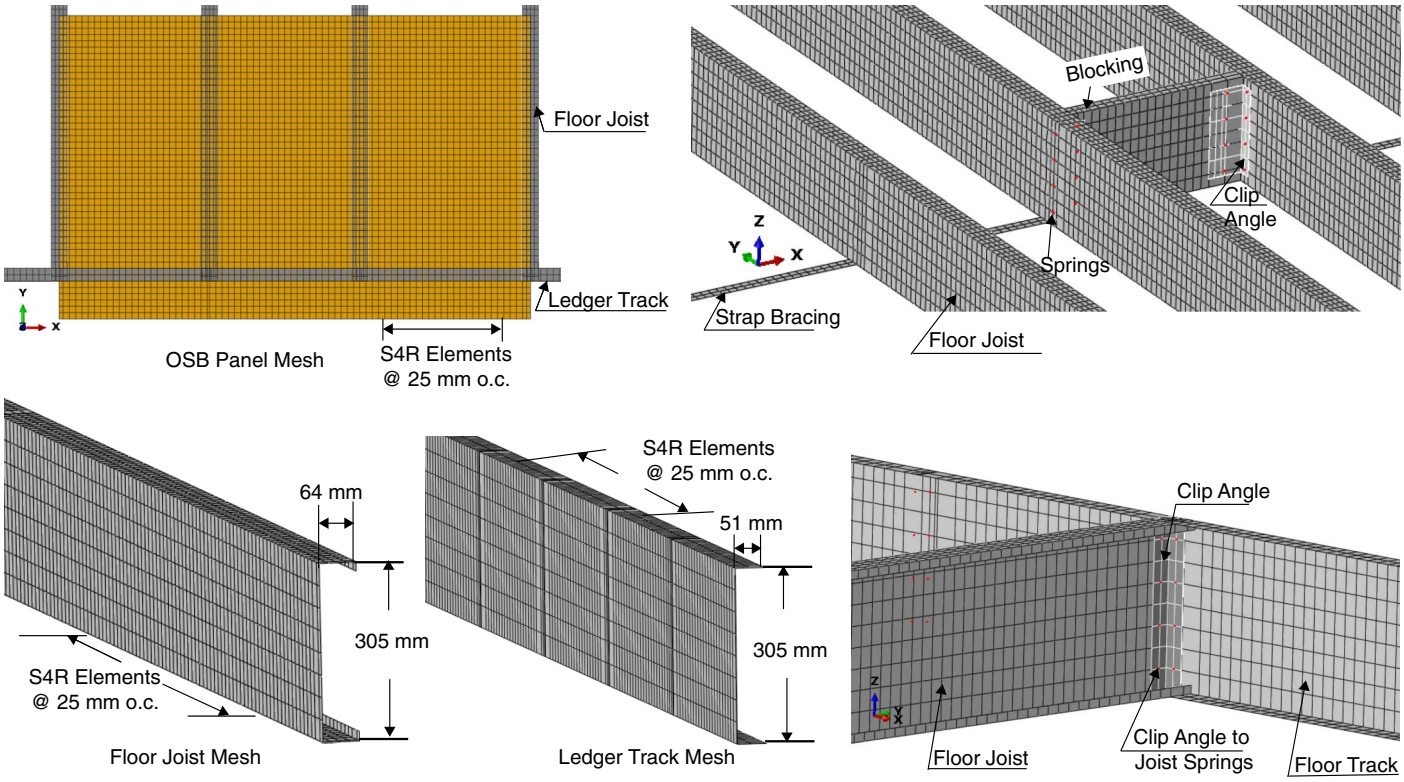

Fig. 4. Modeling of OSB panels, cold-formed steel blocking, joists, tracks, and clip-angles, showing mesh sizes, and spring element locations for screw-fastened connections

with a Poisson's ratio of 0.30. The OSB was modeled as isotropic with an elastic modulus of 2.4 GPa and a Poisson's ratio of 0.30, on the basis of the International Building Code Table 2305.2.2 (ICC 2013) for rated OSB sheathing. The plasticity was modeled in the cold-formed steel joists and tracks by specifying the true plastic strains at increasing true stress levels, starting with zero plastic strain at the beginning of the yield plateau (402 MPa) and culminating at 10% plastic strain at the true ultimate stress 601 MPa (Moen 2008). The initial geometric imperfections in the cold-formed steel members were not modeled because the slender elements (e.g., the joists and tracks) experience minimal compressive stresses and the loading eccentricities trigger second-order out-of-plane deformation.

Modeling Contact and Friction between Tongue-and-Groove OSB Panels

The contact was modeled along all the OSB panel edges (seams) to prevent the adjacent panels from penetrating into each other, using axial springs and displacement constraints. Two adjacent panel edges were connected via axial spring elements (*Spring2* in *ABAQUS*) spaced evenly at 76.2 mm along the edge. These springs have infinite compressive stiffness and zero tensile stiffness, and they prevent panel overlap. Fully blocked (perfect friction) and unblocked (no friction or fasteners) conditions were modeled at the tongue-and-groove seams along the long OSB panel edges. For the fully blocked case, the nodes along the panel edges were constrained to have identical displacements in the shear direction, using the mathematical constraints (**EQUATION* keyword in *ABAQUS*); for the unblocked case, these constraints were released.

Modeling Screw Fastener Load-Deformation Response

The sheathing-to-joist, sheathing-to-track, sheathing-to-wall, joist-to-wall stud, and track-to-wall stud connections were modeled as nonlinear *ABAQUS SpringA* elements in the fastener shear plane and rigid axial couplings in the out-of-plane direction. The *SpringA* elements acted as radial springs and had the capability of rotating in their own plane and updating their configurations in geometrically nonlinear analyses. These springs were assigned the connection load-deformation response parameters shown in Fig. 3, with the average parameter magnitudes provided in Table 1.

Model Solution Algorithm and Boundary Conditions

The equivalent inertial forces in the short direction [degrees of freedom (DOF) 2 or Y in Fig. 2] were assumed to act as a body force distributed across the volume of the sheathing (**DLOAD* in *ABAQUS*). The load was applied statically, ignoring inertia effects, with a large-displacement (nonlinear geometric) formulation. The solution algorithm solved simultaneously for forces and displacements at each analysis step to achieve convergence during the softening response (the Riks method, implemented as **STATIC, Riks* in *ABAQUS*). The building lateral force-resisting system that framed the boundary of the diaphragm was idealized to have infinite in-plane stiffness and negligible out-of-plane stiffness. To achieve this in the model, the long-direction boundary nodes (shown in Fig. 5 as dots on the north and south diaphragm edges) were restrained translationally in the long floor direction (shown following X in the Fig. 5 coordinate system), and the short-direction boundary nodes (in Fig. 5, at the west and east diaphragm edges) were restrained in the short floor direction (shown following Y in the Fig. 5 coordinate system). All the boundary nodes were also restrained in the vertical direction (DOF 3 or Z). The edge joists, ledger tracks, and sheathing connected to the boundary nodes via the *SpringA* elements and axially rigid links, as shown in Fig. 5.

Floor Diaphragm Load Path Mappings from High-Fidelity Simulation

The floor diaphragm model can be used to study the flow of the in-plane diaphragm forces from the sheathing and cold-formed steel framing into the building lateral system. For the blocked diaphragm case, the in-plane diaphragm forces are carried in the OSB as a shear element to the double-shear sheathing-to-wall connections (Fig. 2), and the field fastener forces are minimal, as shown in Fig. 6(a). For the unblocked diaphragm case, the OSB sheathing is less effective and the field fasteners experience up to 100% higher demands as they transfer the in-plane forces from OSB panel to OSB panel; see Fig. 6(b). The unblocked edges result in a lower system capacity because the field fasteners fracture first, a phenomenon that was also observed in the full-scale diaphragm test (Florig et al. 2016). The blocked diaphragm load paths follow classical assumptions where the diaphragm is idealized as a deep beam with flexural force demands at its chords (the long edge) and shear force demands at the collectors (the short edge). The force flow in the unblocked diaphragm does not follow the classical assumptions and can be captured only by high-fidelity finite-element simulations. The diaphragm load paths affect the global system response and reliability, as discussed next.

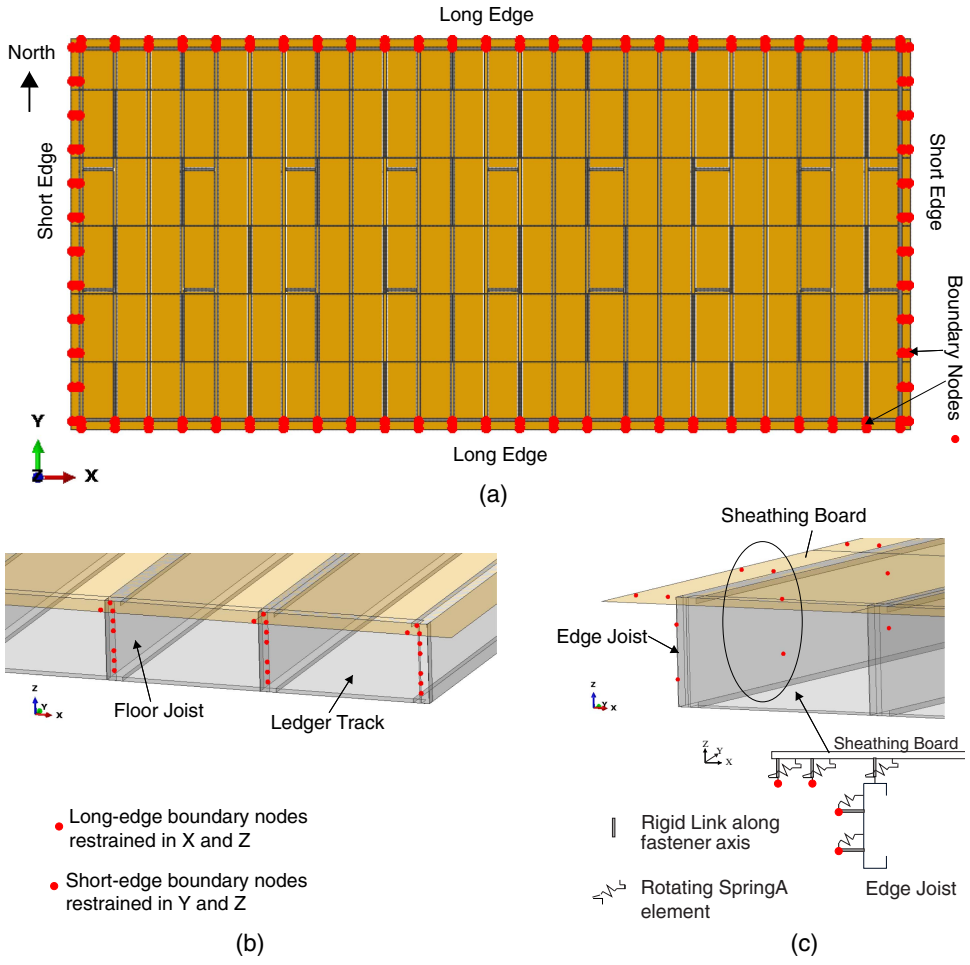

Fig. 5. High-fidelity wood-sheathed cold-formed steel-framed floor diaphragm model: (a) plan view showing OSB panels and underlying framing with dots representing nodes to which boundary conditions are applied; (b) view along the diaphragm long direction including ledger track and clip angle connections to the joists; (c) view along the diaphragm short direction showing edge joists attached to boundary nodes through framing-to-wall connections

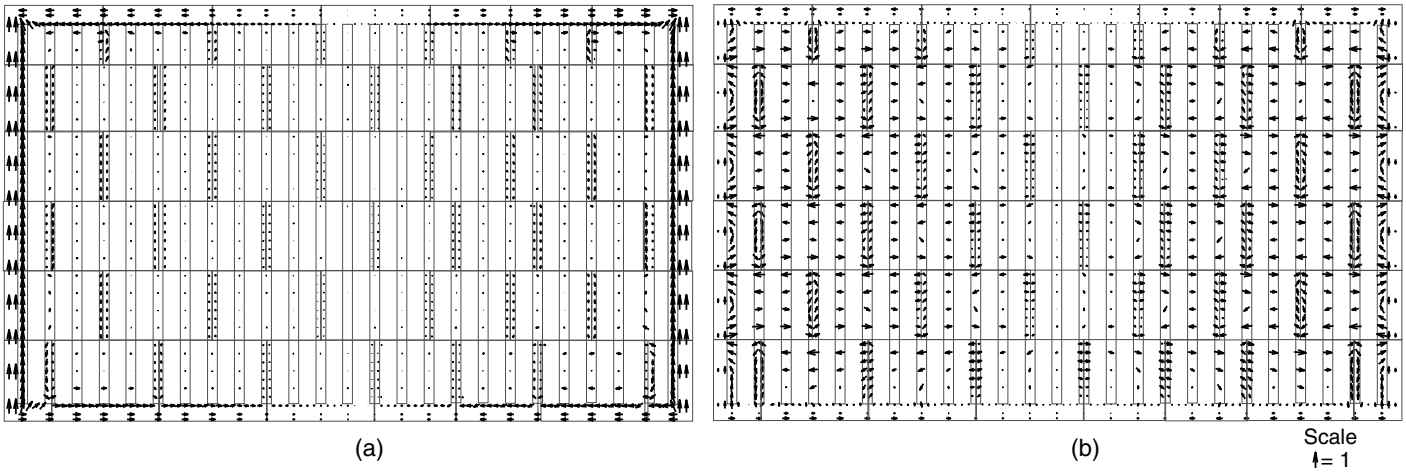

Fig. 6. Fastener demand to capacity vectors (D_i/C_i) scaled to magnitude in shear at diaphragm system failure considering (a) blocked and (b) unblocked panel edges; field fastener demand-to-capacity ratios are higher in the unblocked case because OSB panels slide against each other, requiring the underlying steel framing to carry in-plane forces

With all the diaphragm details modeled, an in-plane body force was applied on the OSB panel elements, resulting in the global floor response shown in Fig. 7. For the blocked diaphragm case (i.e., the OSB tongue-and-groove panel seams are constrained together), the load-deformation response was nonlinear because the fastener connection response was nonlinear (Fig. 8), and the peak load of $C_{sys} = 711$ kN (6.7 kN/m^2 multiplied by the floor diaphragm area of 106 m^2 equivalent to 47 kN/m along the diaphragm long edge) was reached as the double-shear sheathing-to-wall connections experience a cascading brittle failure. Note that the connections that were designed to carry lateral loads were the sheathing-to-edge joist connections shown in Fig. 2, whereas the sheathing-to-wall connections where failure initiated were not a designed load path to the lateral system.

For the unblocked case (where the friction at the OSB panel seams was assumed as zero), the initial stiffness was reduced 85% in comparison with the blocked diaphragm because the in-plane shear stiffness continuity was lost (39 to 6.2 kN/mm secant stiffness from 0 to 8 mm). This required the underlying framing to carry the in-plane loads from OSB panel to OSB panel until the loads reached the lateral system. The system failure mode also changed, shifting from the diaphragm–shear wall interface to the field fasteners along the panel seams as they slid relative to one another, resulting in an 80% decrease in the diaphragm system capacity (711–181 kN, as shown in Fig. 7). These results highlight the valuable load path and limit-state information that high-fidelity modeling can provide.

A full-scale experiment was recently completed on the same wood-sheathed cold-formed steel framed diaphragm configuration considered here (Florig et al. 2016), with loads applied at the quarter points with a drag strut connected between two joists. A frictional coupling spring with a stiffness of 0.003 kN per mm of contact (Chatterjee et al. 2017) between all the long-edge panel seams was incorporated in the simulation. The measured and simulated response (with identical load patterns applied at the quarter points with drag struts) shown in Fig. 7 confirmed the viability of the high-fidelity model and demonstrated that the as-constructed

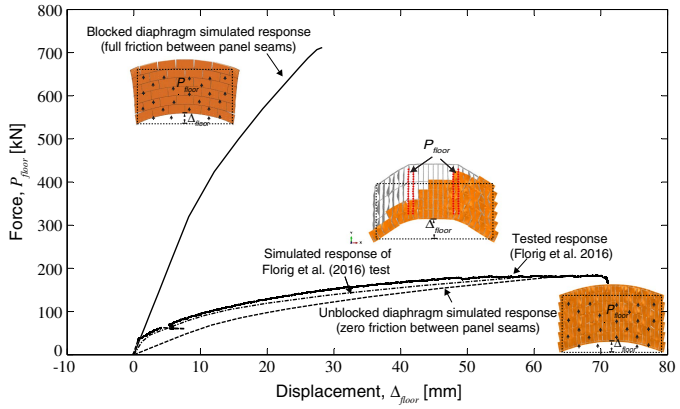

Fig. 7. Simulated wood-sheathed cold-formed steel floor diaphragm load-deformation response is 85% stiffer and 80% stronger when considering perfect friction between panel seams (i.e., a blocked diaphragm configuration) when compared to frictionless (unblocked) seams, verified with a comparison between diaphragm response due to uniform loads applied at joists symmetrically about mid-span (Florig et al. 2016) and computational response with partial inter-panel friction included

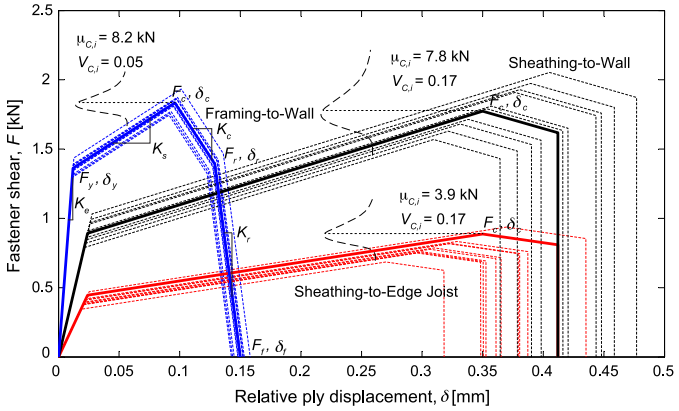

Fig. 8. Sheathing-to-wall, sheathing-to-edge joist and framing-to-wall screw fastener connection models with baseline (deterministic) response and random realizations of fastener peak shear (F_c) with stiffness maintained constant in each linear segment

diaphragm panel seams were closer to unblocked than to blocked. With this knowledge about the relationship between the structural details, the load paths, and the limit states in hand, the diaphragm system reliability can next be quantified and explored.

Wood-Sheathed Cold-Formed Steel Framed Diaphragm System Reliability

The availability of the floor diaphragm force distribution from the high-fidelity simulations makes it possible to quantify the demand magnitudes of the critical components, of which, in this case, the OSB fastener connections are of great interest. The fastener connection reliabilities are correlated through the diaphragm load-sharing network and define the probability of the system failure $P(C_{\text{sys}} \le D_{\text{sys}})$, that is, its system reliability.

Diaphragm System Reliability Calculation Approach

Structural system reliability may be written in the form of a reliability index β_{sys}

$$\beta_{\text{sys}} = -\Phi^{-1}[P(C_{\text{sys}} \le D_{\text{sys}})] \tag{1}$$

where Φ = standard normal cumulative distribution function; C_{sys} and D_{sys}, = random variables denoting system capacity and system demand; and $P(C_{\text{sys}} \le D_{\text{sys}})$ denotes the probability of system failure.

The probability $P(C_{\text{sys}} \le D_{\text{sys}})$ can be calculated numerically with a convolution approach if the distributions C_{sys} and D_{sys} are known or assumed (Ross 1995)

$$P(C_{\text{sys}} \le D_{\text{sys}}) = \int_{d=0}^{\infty} P(C_{\text{sys}} \le d | D_{\text{sys}} = d) P(D_{\text{sys}} = d) = \int_{d=0}^{\infty} P(C_{\text{sys}} \le d | D_{\text{sys}} = d) P(D_{\text{sys}} = d) \tag{2}$$

The numerical integration varies over discrete steps on the interval d, spanning the range of the C_{sys} and D_{sys} distributions. In the case of this diaphragm study, d has units of kN, and the objective is to estimate the probabilistic distribution of C_{sys} using stochastic simulations on an experimentally verified high-fidelity finite-element model.

Calculating Diaphragm System Capacity, C_{sys}

The diaphragm system capacity distribution C_{sys} is obtained by performing stochastic simulations to the diaphragm failure with the modeling protocol presented and verified previously, where failure is defined as the peak load reached. Each realization for the floor diaphragm model includes randomly sampled fastener load-deformation model parameters. All the other diaphragm structural components (e.g., the cold-formed steel joists and OSB sheathing shear stiffness) are treated with deterministic properties.

Randomness in the diaphragm screw-fastened sheathing-to-wall, sheathing-to-edge joist, sheathing-to-ledger track, framing-to-wall fastener, and sheathing-to-framing field fastener connections is imposed in the diaphragm system simulations with the multilinear fastener models shown in Fig. 8. The capacity F_c^i of fastener $i = 1$–405 are sampled as independent and identically distributed random variables, assuming a lognormal distribution with the mean and COV of $\mu_{C,i}$ and $V_{C,i}$, respectively. The fastener connection stiffness is assumed to stay constant in the four response branches such that the remaining quadrilinear parameters scale linearly with F_c^i, that is, $F_y^i = F_c^i F_y / F_c$, $F_r^i = F_c^i F_r / F_c$, $\delta_y^i = F_c^i \delta_y / F_c$, $\delta_c^i = F_c^i \delta_c / F_c$, $\delta_r^i = F_c^i \delta_r / F_c$, and $\delta_f^i = F_c^i \delta_f / F_c$. Fig. 8 shows as dotted lines the example sets of 10 randomly generated fastener-response realizations.

Fig. 9 shows the histogram of C_{sys} for the blocked and unblocked diaphragm cases, each generated with 100 realizations. The mean of C_{sys} ($\mu_{C\text{sys}} = 644$ kN blocked and $\mu_{C\text{sys}} = 176$ kN unblocked) is modestly less than the simulated deterministic strengths (assuming all fasteners have the mean response shown in Fig. 8), because the weakest fastener in each random simulation initiates the redistribution earlier. The variability in C_{sys} is higher in the unblocked diaphragm ($V_{C\text{sys}} = 3.3\%$ for unblocked versus $V_{C\text{sys}} = 2\%$ for blocked) because there are more field fasteners sampled that have an impact on the response. Overall, the system variability is significantly less than the input fastener variability of 17%, a trend also observed for the cold-formed steel shear walls (Bian et al. 2017), which represents the beneficial system effect available in repetitive construction. The variability from modeling uncertainty was minimized by using a comprehensively validated finite-element modeling protocol for the thin-walled cold-formed steel structural components (Schafer et al. 2010; Moen and Schafer 2009) that results in a simulated-to-tested coefficient of variation less than 5%.

Calculating Diaphragm System Demand, D_{sys}

The in-plane diaphragm system demand varies with the loading type (seismic or wind) and the building configuration. In this study, a seismic equivalent lateral force (ELF) is considered on the CFS-NEES building (Fig. 1). The distribution for D_{sys} is assumed lognormal consistent with the load and the resistance factor design (LRFD) implementation (Lin et al. 1988), and D_{sys} represents the total inertial force on the diaphragm.

The mean diaphragm system demand, $\mu_{D\text{sys}} = 114$ kN, is obtained from the implicit dynamic analysis results from a spring-based building model (Chatterjee 2016) subjected to 44 ground motion records scaled to the design basis earthquake level (ATC 2009). The building model treats each shear wall and diaphragm as a nonlinear spring. The shear wall force-deformation response is obtained from the subsystem experimental results (Liu et al. 2014). Diaphragm force-deformation relationships are modeled in a manner consistent with the experimentally calibrated finite-element model results shown in Fig. 7, the simulated response of Florig et al. (2016) test. The same model with the coupling friction released (in Fig. 7, the unblocked diaphragm simulated response) is used for the diaphragm subsystem capacity calculations subsequently in this paper. The mean diaphragm system demand, $\mu_{D\text{sys}}$, is consistent with the CFS-NEES building shake-table measurements and simulations (Schafer et al. 2016; Peterman 2014).

The variation in this ELF diaphragm seismic demand is assumed to be $V_{D\text{sys}} = 0.38$, corresponding to the ASCE 7-10 load combination $1.2D + 1.0L + 0.2S + 1.0E$ (ASCE 2010), where D is the dead load, L is the live load, S is the snow load, and E is the earthquake load, for California. The coefficient of variation $V_{D\text{sys}}$ is obtained from a first-order second-moment reliability parameter study (Meimand and Schafer 2014) that demonstrated that $V_{D\text{sys}}$ was as much as 75% higher for the load combinations including earthquakes than for a typical $D + L$ combination.

Fig. 9 shows a plot of the D_{sys} distribution, which accommodates a direct comparison with C_{sys} for the blocked and unblocked diaphragm configurations. The blocked diaphragm had a large reserve capacity, $C_{\text{sys}} \gg D_{\text{sys}}$, because the current strength design approach in the AISI S240 North American Standard for Cold-Formed Steel Framing (AISI 2015b), used to define the fastener quantities, diameter, and patterns for the CFS-NEES building, uses

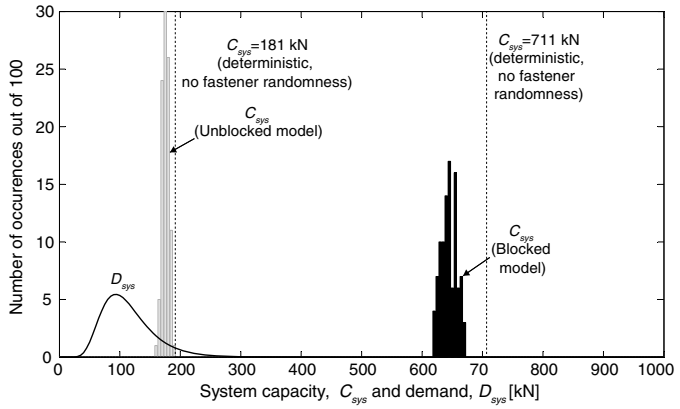

Fig. 9. Diaphragm system capacity (C_{sys}) and demand (D_{sys}) distributions, where C_{sys} is calculated using stochastic simulation and D_{sys} is calculated from nonlinear dynamic simulations on a full-building CFS-NEES model with 44 ground motions (Chatterjee 2016; ATC 2009). Mean C_{sys} is less than the deterministic capacity because the weakest fastener causes a cascading system failure

the lower-bound test results for the sheathing-to-steel connection strength. The mean unblocked diaphragm capacity was 35% higher than the mean seismic demand ($\mu_{C\text{sys}} = 176$ kN versus $\mu_{D\text{sys}} = 114$ kN).

Calculating Diaphragm System Reliability, β_{sys}

The distribution shape, statistics, and overlap of D_{sys} and C_{sys} define the probability of system failure. The C_{sys} histogram shown in Fig. 9 was approximated with a lognormal distribution using $\mu_{C\text{sys}} = 644$ kN and $V_{C\text{sys}} = 2\%$ for the blocked diaphragm and using $\mu_{C\text{sys}} = 176$ kN and $V_{C\text{sys}} = 3.3\%$ for the unblocked diaphragm. These distributions were used in Eq. (2), which was numerically integrated over the limits $d = 0$ to 1,200 kN, resulting in $P(C_{\text{sys}} <= D_{\text{sys}}) = 5\text{e-}7$ for the blocked diaphragm and $P(C_{\text{sys}} <= D_{\text{sys}}) = 0.09$ for the unblocked diaphragm, corresponding to a β_{sys} of 4.9 and 1.4, respectively. The probability of a system failure $P(C_{\text{sys}} <= D_{\text{sys}})$ is approximately 30% higher (e.g., $\beta_{\text{sys}} = 1.4$ versus 1.2 for unblocked) if no system benefit is considered (i.e., if $V_{C\text{sys}} = V_{C,i}$); this benefit is taken advantage of in a design context in the following example.

Simulation-Enabled Structural Design to a System Reliability Target

Whereas most structural design codes follow a component reliability–based procedure, the more common goal of designers is to ensure the acceptable failure probabilities for a group of components and connections that work together as a structural system. The target system reliability index $\beta_{t,\text{sys}}$ that reflects this goal can be related to the system damage and failure consequences, for example, the life safety and repair costs. The following approach and example show how the structural component reliabilities and their correlation to the load paths and load-deformation response can be defined to meet a specific system-reliability target.

The reliability β_i of the component or connection i in a structural system (Fig. 10) is correlated to the system reliability β_{sys}. In general, the relationship between the component and system reliability is not available analytically; however, with the advances in structural simulation such as those introduced and verified here, the sensitivity of system reliability to changes in component reliability reflecting the load path and redundancy become available. This sensitivity $S_{\beta,i}$ for component i is defined as $S_{\beta,i} = \partial\beta_{\text{sys}}/\partial\beta_i$, where $S_{\beta,i}$ represents the change in the system reliability as the reliability of one component or connection in the system, β_i, is perturbed.

An approach for finding the vector of component reliabilities in a system, $\{\beta\}$, that produces $\beta_{\text{sys}} = \beta_{t,\text{sys}}$ begins by establishing an initial design for all the components and connections, for example, with a code-based component-level LRFD approach. The system reliability sensitivity vector for each component and connection $\{S_\beta\}$ is obtained from the system simulations of this initial design. The component or connection m that has the highest influence on the system reliability is identified, i.e., $S_{\beta,m} = \max\{S_\beta\}$, and then its reliability is modified as $\beta_m^* = \beta_m + (\beta_{t,\text{sys}} - \beta_{\text{sys}})/S_{\beta,m}$. Then the component m is excluded from the set and the procedure is repeated across all other components. The solution converges to $\{\beta\} = \{\beta^*\}$ if $\beta_{\text{sys}} = \beta_{t,\text{sys}}$ and $\{\beta^*\}$ is acceptably low or cannot be lowered further without making $\beta_{\text{sys}} < \beta_{t,\text{sys}}$. If convergence is not achieved, that is, $\beta_{\text{sys}} \neq \beta_{t,\text{sys}}$ or $\{\beta^*\}$ can be reduced further,

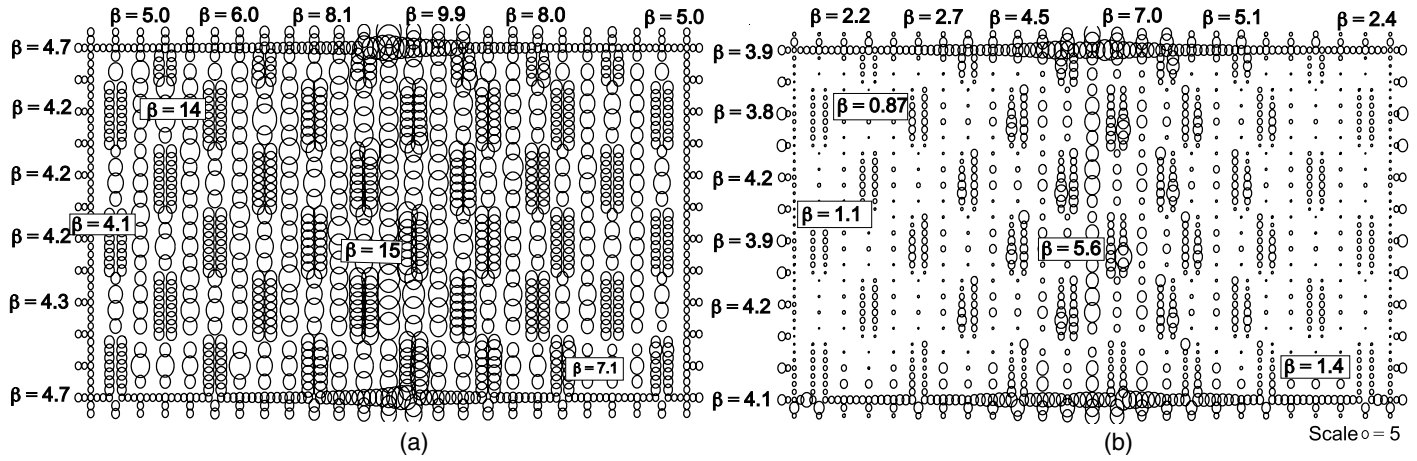

Fig. 10. Fastener reliabilities at a diaphragm demand of 114 kN for (a) blocked diaphragms; (b) unblocked diaphragms, with circle radii scaled to the reliability index at that location

the algorithm is restarted from the most sensitive component or connection.

Convergence to $\beta_{t,\text{sys}}$ is achieved quickly for the systems with a weak link or a single load path. However, for the redundant systems with a large number of components and connections having a comparable β_i, the iterations to converge to $\beta_{\text{sys}} = \beta_{t,\text{sys}}$ require on the order of n iterations, where n is the number of system components and connections. The iterations and associated simulations to obtain $\{S_\beta\}$ and β_{sys} can be reduced by treating the groups of related components together and by changing the reliabilities as a group in calculating the $\{S_\beta\}$ and β_{sys}. This reduced-order approach is applied to the diaphragm shown in Fig. 1 as a system-reliability design example in the following section.

Cold-Formed Steel-Framed Diaphragm System Reliability Design Example

For this example, the floor diaphragm system reliability was assumed to be defined by two groups of screw fasteners, sheathing-to-joist field fasteners, and sheathing-to-wall plus sheathing-to-edge joist fasteners, for both the unblocked and the blocked panel edge conditions. The fastener initial designs, e.g., the size and spacing, were obtained from AISI S213-07 (AISI 2007b), now superseded by AISI S400-15 (AISI 2015a), as documented in the design narrative for the CFS-NEES building (Madsen et al. 2011). The resulting reliability of fastener i was estimated as

$$\beta_i = \frac{\ln \frac{\mu_{C,i}}{\mu_{D,i}}}{\sqrt{V_{C,i}^2 + V_{D,i}^2}} \tag{3}$$

where $\mu_{C,i}$ = mean fastener capacity assumed as peak connection strength F_c (Fig. 8 and Table 1); and $V_{C,i} = 0.165$ for all sheathing-to-framing fasteners and $V_{C,i} = 0.048$ for framing-to-wall fasteners (Tao et al. 2016). The fastener demands were obtained from simulation (Fig. 6) at the mean system demand level $\mu_{D\text{sys}} = 114$ kN with $V_{D,i} = 0.38$, resulting in the diaphragm fastener reliability distribution shown in Fig. 10. The assumed fastener demand variability was for an elastic load-sharing network that in reality decreased due to inelasticity.

For the initial code-based design, in the blocked diaphragm, the fastener reliability β_i was lowest at the sheathing-to-wall connections where the demand loads collected ($\beta_{\text{edge,min}} = 4.1$), and increased in the field of the diaphragm ($\beta_{\text{field,min}} = 7.1$). In the unblocked diaphragm, the fastener reliabilities were lowest in the diaphragm field ($\beta_{\text{field,min}} = 0.87$), with higher edge fastener reliabilities ($\beta_{\text{edge,min}} = 1.1$) because the underlying steel framing resisted the in-plane panel deformation with a cumulative total force magnitude of 967 kN resulting from a 114-kN mean demand to the lateral systems, compared with 67 kN in the blocked diaphragm case. This meant that an applied shear load caused flexural deformation and rigid body rotation in each individual panel, which in the unblocked diaphragm case led to the magnified individual force magnitudes perpendicular to the applied force direction. These force magnitudes canceled each other out, leading to a resultant sum of zero, but caused high force demands on each individual connection element.

The baseline reliabilities obtained for the original system designed with the standard component LRFD were $\beta_{\text{sys}} = 4.9$ and $\beta_{\text{sys}} = 1.4$ for the blocked and unblocked diaphragms, respectively. It was assumed that a target $\beta_{t,\text{sys}} = 2.1$ was needed to achieve a total building system reliability of $\beta_{t,\text{building}} = 2.5$ for the CFS-NEES building (Chatterjee 2016), where $\beta_{t,\text{building}}$ was established as the building collapse probability for a design basis earthquake of 0.006 consistent with recommendations from FEMA-P695 that the acceptable collapse probability for a 1/5 as frequent maximum considered earthquake is 0.1 (ATC 2009). This was numerically equivalent to the member target reliability used in the LRFD but was not otherwise related to it in terms of the component-to-system reliability.

Table 2. System Reliability Sensitivity Iterations for the Unblocked Floor Diaphragm

Iteration number	$\beta_{\text{edge,min}}$	$\beta_{\text{field,min}}$	$S_{\beta,\text{edge}}$	$S_{\beta,\text{field}}$	C_{sys} (kN)	β_{sys}
1	1.1	0.90	0.20	0.88	176	1.4
2	1.1	1.8	0.38	—	229	2.1

Table 2 and Fig. 11(a) summarize the resulting reliability sensitivity solution for the unblocked diaphragms, with convergence occurring after 2 iterations. The algorithm began by perturbing the baseline $\beta = [\{\beta_{\text{edge}}\}\{\beta_{\text{field}}\}]$, resulting in $\{S_\beta\} = \{S_{\beta,\text{edge}} S_{\beta,\text{field}}\} = \{0.20 \quad 0.88\}$ [see iteration (1) shown in Fig. 11(a) and Table 2] and $S_{\beta,m} = \max\{S_\beta\} = 0.88$, where component group m is the set of field fasteners. For the edge fasteners that comprised the sheathing-to-wall and sheathing-to-joist connections, F_c was perturbed from 7.8 to 9.4 kN (a change of 1.6 kN) and from 3.9 to 4.7 kN (a change of 0.8 kN), respectively, with the fastener model stiffness and variability $V_{C,i}$ unchanged. This approximately equaled increasing the fastener size from #10 to #12, which is a common choice for the sheathing and steel thicknesses used here. For the field fasteners, F_c was perturbed from 3.9 to 4.7 kN. The perturbation size was chosen to be small enough to ensure that $\{S_\beta\}$ remained constant; see the start and end points for the reliability sensitivity iterations shown in Fig. 11(a).

The updated fastener reliabilities for the unblocked diaphragm were calculated $\beta_m^* = \beta_m + (\beta_{t,\text{sys}} - \beta_{\text{sys}})/S_{\beta,m} = 1.8$, and β_{sys} became equal to the value of $\beta_{t,\text{sys}}$, i.e., 2.1. The reliability sensitivity for the edge fasteners was computed $S_{\beta,\text{edge}} = 0.38$, and because its sensitivity was nonzero and positive, the edge fastener reliability could not be reduced for savings without making $\beta_{\text{sys}} < \beta_{t,\text{sys}}$. The values of $\{\beta_{\text{edge,min}} \quad \beta_{\text{field,min}}\} = \{1.1 \quad 1.8\}$ shown in Fig. 11(a), iteration (2), were thus the minimum component reliabilities to provide $\beta_{t,\text{sys}} = 2.1$ for the diaphragm. Following the same approach for blocked diaphragms as summarized in Table 3 and shown by Fig. 11(b), iteration (1), $\{S_\beta\} = \{S_{\beta,\text{edge}} S_{\beta,\text{field}}\} = \{1.10\}$; that is, the system reliability was insensitive to the field fastener strength because the shear transfer from OSB panel to OSB panel was achieved through friction. The fastener reliabilities were updated first by perturbing the edge fastener reliability in iteration (2) and then the field fastener reliability in iteration (3), leading to $\{\beta_{\text{edge,min}} \quad \beta_{\text{field,min}}\} = \{1.6 \quad 1.6\}$ and $\beta_{\text{sys}} = \beta_{t,\text{sys}} = 2.1$, which was accepted as a converged solution.

The variation in the system reliability β_{sys} with the fastener reliability β_{edge} and β_{field} shown in Fig. 11(b) highlights how the choices made for the reliability of the fastener groups can affect the controlling system-strength limit state. The system reliability increases linearly in the blocked diaphragm with the edge fastener reliability (i.e., the system strength increases linearly with the edge fastener strength) until the system-strength limit state shifts to the edge joist-to-wall connections. Beyond this limit-state transition, increasing the sheathing-to-wall fastener component reliability no longer improves the system reliability. Solving for $\mu_{c,i}$ in Eq. (3) with $\beta_i = \beta_{\text{edge}}$ or β_{field} taken from the final iteration presented in Table 2 or Table 3, the required fastener design capacities to reach $\beta_{\text{sys}} = 2.1$ for the blocked diaphragm were 1.4 kN at the edge and 0.52 kN in the field (i.e., increasing the fastener spacing at the wall

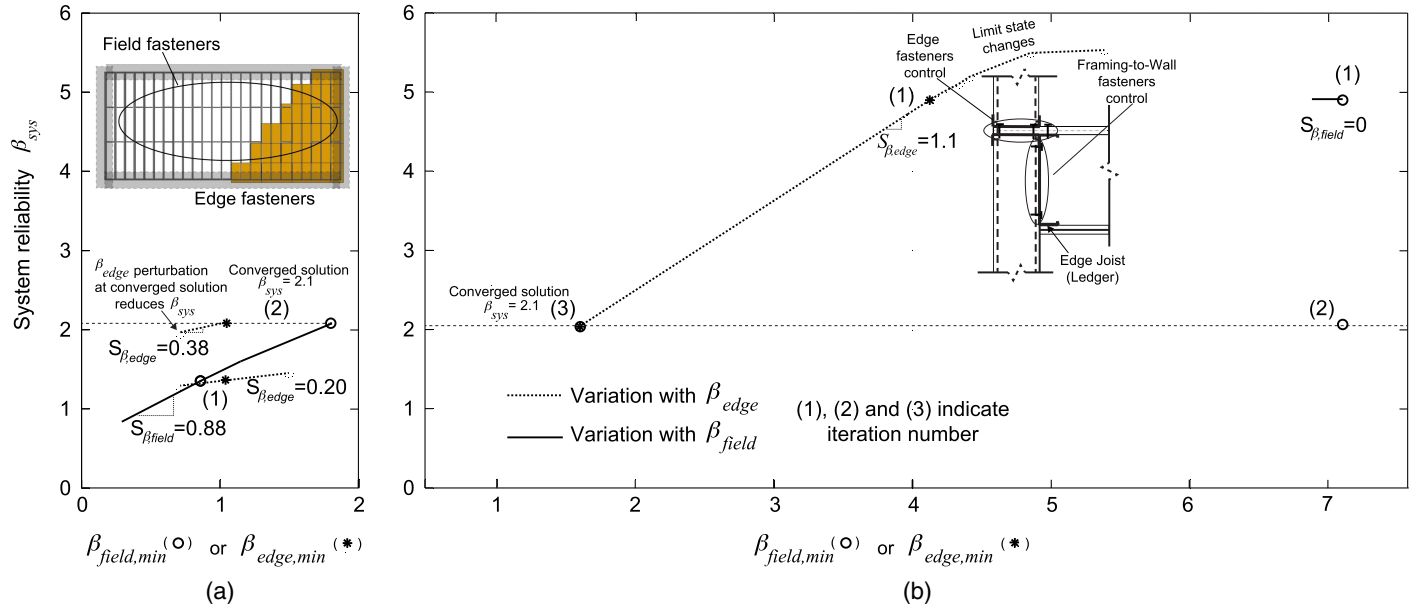

Fig. 11. Diaphragm system reliability increases with (a) field fastener reliability ensuring shear continuity at panel seams for unblocked diaphragms; (b) edge fastener reliability connecting the diaphragm to the lateral system for blocked diaphragms

Table 3. System Reliability Sensitivity Iterations for the Blocked Floor Diaphragm

Iteration number	$\beta_{\text{edge,min}}$	$\beta_{\text{field,min}}$	$S_{\beta,\text{edge}}$	$S_{\beta,\text{field}}$	C_{sys} (kN)	β_{sys}
1	4.1	7.1	1.1	0	644	4.9
2	4.1	7.1	—	0	227	2.1
3	4.1	1.6	—	0	226	2.1

edge from 152 to 432 mm), and 3.9 kN at the edge and 5.8 kN in the field for the unblocked diaphragm (decreasing the fastener spacing at the panel seams from 152 to 102 mm).

The fastener group reliabilities presented in Tables 2 and 3, i.e., $\{\beta_{\text{edge}}\ \beta_{\text{field}}\}=\{1.1\ 1.8\}$ for the unblocked and $\{\beta_{\text{edge}}\ \beta_{\text{field}}\}=\{1.6\ 1.6\}$ for the blocked diaphragms that resulted in $\beta_{\text{sys}}=2.1$ can be represented in an LRFD design context by calculating the fastener group resistance factor ϕ

$$\varphi = \frac{M_m F_m P_m}{B} e^{-\beta\sqrt{V_C^2+V_D^2}} \tag{4}$$

where $\beta=\beta_{\text{edge}}$ for the edge fasteners; and $\beta=\beta_{\text{field}}$ for the field fastener components. Calculating Eq. (4) consistent with current the AISI practice: $M_m=1.1$, $F_m=P_m=1.0$ from AISI S100-16, Chapter F (AISI 2016), and $V_C=0.17$ from Table 1 (COV of F_c). The assumed ratio of the mean demand to the code-specified demand, i.e., the load bias, was $B=1.0$.

Resistance factors for the unblocked diaphragm were $\phi=0.81$ (edge fasteners) and $\phi=0.68$ (field fasteners), and for the blocked diaphragm $\phi=0.71$ for both field and edge fasteners, assuming $V_D=0.21$ dead + live load variability is applicable for a seismic-load case. Alternatively, considering the seismic load variability at the fastener level, i.e., $V_D=V_{D\text{sys}}=0.38$, $\phi=0.70$ (edge fasteners) and $\phi=0.52$ (field fasteners), and for the blocked diaphragm $\phi=0.57$ for both the field and the edge fasteners in the unblocked diaphragm. Applying the resistance factors to the field fasteners for the unblocked diaphragm, the demand of 2.8 kN divided by $\phi=0.52$ and multiplied by $M_m=1.1$ resulted in 5.8 kN, which was the fastener capacity determined previously to reach $\beta_{\text{sys}}=2.1$ for the diaphragm. It is hypothesized that the fastener demand variability is dampened by load redistribution (i.e, $V_D<0.38$), and the range of resistance factors presented here attempts to bound the LRFD application to the seismic system reliability as research continues in this area.

Conclusion

A structural system design approach was presented that considered component and connection reliability, load paths, force flow, and redundancy with high-fidelity computational simulations, in order to provide system reliability quantification. The simulations provided a means for calculating the system reliability sensitivity to component and connection design, and the sensitivity guided an iterative solution to determine the component reliabilities (and the associated resistance factors) that met a system reliability target.

The system reliability design approach was applied to a wood-sheathed cold-formed steel framed floor diaphragm supported by stochastic simulations to system collapse that considered screw fastener load-slip response variability. The system performance and reliability for unblocked wood-sheathed cold-formed steel framed diaphragms was most sensitive to the field fastener load-slip response, and in blocked diaphragms the edge fasteners connecting the sheathing to the lateral system dominated the system response and probability of failure.

The system reliability calculation approach was used here to design a sheathed cold-formed steel framed floor diaphragm; however, it is just as applicable to other structural systems and construction materials and even to full buildings if the verified high-fidelity collapse simulation protocols of important subsystems (the shear walls and diaphragm) are available along with accurate load-distribution models. It is envisioned that the design-to-system reliability targets can be applied archetype-by-archetype in the codes and standards by identifying the general correlation trends between the component and connection groups and the system reliability, and then codifying these trends as component group resistance

factors that take advantage of the beneficial system effects when redundancy is high and that warn engineers and penalize efficiency when they have designed a weakest-link system.

Acknowledgments

This material is based upon work supported by the National Science Foundation under Grants 1301001 (Virginia Tech), 1301033 (University of Massachusetts, Amherst), and 1300484 (Johns Hopkins University). Any opinions, findings, and conclusions or recommendations expressed in this material are those of the authors and do not necessarily reflect the views of the National Science Foundation. The authors are grateful to their industry partner, the American Iron and Steel Institute, for their cooperation, and to Virginia Tech Advanced Research Computing for the supercomputing resources used in the finite element simulations.

References

ABAQUS version 6.13 [Computer software]. Dassault Systèmes, Waltham, MA.

AISI (American Iron and Steel Institute). (2007a). "Commentary on S213-07 (North American standard for cold-formed steel framing—Lateral design)." *AISI S213-07 Commentary*, Washington, DC.

AISI (American Iron and Steel Institute). (2007b). "North American standard for cold-formed steel framing: Lateral design." *AISI S213-07*, Washington, DC.

AISI (American Iron and Steel Institute). (2012a). "Commentary on North American cold-formed steel specification for the design of cold-formed steel structural members." *AISI S100-12 Commentary*, Washington, DC.

AISI (American Iron and Steel Institute). (2012b). "North American specification for the design of cold-formed steel structural members." *AISI S100-12*, Washington, DC.

AISI (American Iron and Steel Institute). (2015b). "North American standard for cold-formed steel structural framing." *AISI S240-15*, Washington, DC.

AISI (American Iron and Steel Institute). (2015a). "North American standard for seismic design of cold-formed steel structural systems." *AISI S400-15*, Washington, DC.

AISI (American Iron and Steel Institute). (2016). "North American specification for the design of cold-formed steel structural members." *AISI S100-16*, Washington, DC.

ANSI/NFoPA (American Forest and Paper Association/American Iron and Steel Institute). (1991). "NDS 1991: National design specification for wood construction." *NDS 1991*, Leesburg, VA.

APA (The Engineered Wood Association). (2011). "Performance rated panels: Product guide." Tacoma, WA.

ASCE. (2010). "Minimum design loads for buildings and other structures." *ASCE/SEI 7-10*, Reston, VA.

ATC (Applied Technology Council). (2009). "Quantification of building seismic performance factors." *FEMA P695*, Redwood City, CA.

Bian, G., Chatterjee, A., Buonopane, S. G., Arwade, S. R., Moen, C. D., and Schafer, B. W. (2017). "Reliability of cold-formed steel framed shear walls as impacted by variability in fastener response." *Eng. Struct.*, 142(Jul), 84–97.

Chatterjee, A. (2016). "Structural system reliability with application to light steel-framed buildings." Ph.D. dissertation, Virginia Polytechnic Institute and State Univ., Blacksburg, VA.

Chatterjee, A., Rogers, C. A., and Moen, C. D. (2017). "High-fidelity monotonic and cyclic simulation of a wood-sheathed cold-formed steel framed floor diaphragm." *Proc., 16th World Conf. on Earthquake Engineering*, Earthquake Engineering Research Institute, Oakland, CA.

Chatterjee, A., Xiang, Y., Moen, C. D., Arwade, S. R., and Schafer, B. W. (2014). "Towards quantifying beneficial system effects in cold formed steel wood-sheathed floor diaphragms." *22nd Int. Specialty Conf. on Cold-Formed Steel Structures*, Wei-Wen Yu Center for Cold-Formed Steel Structures, St. Louis, MO.

Countryman, D. (1954). "Horizontal plywood diaphragm tests: Full report." *Laboratory Rep. 55*, Douglas Fir Plywood Association, Tacoma, WA.

Ellingwood, B. R., and Galambos, T. V. (1982). "Probability-based criteria for structural design." *Struct. Saf.*, 1(1), 15–26.

Florig, S., Chatterjee, A., O'Brien, P., and Moen, C. D. (2016). "Full scale tests on a cold-formed steel floor diaphragm with oriented strand board sheathing." *Rep. CE/VPI-ST-16/02*, Virginia Tech Structural and Engineering Materials, Blacksburg, VA.

Galambos, T. V. (1990). "System reliability and structural design." *Struct. Saf.*, 7(2–4), 101–108.

Ghosn, M., and Moses, F. (1998). "Redundancy in highway bridge superstructures." *NCHRP Rep. 406*, Transportation Research Board, Washington, DC.

Hendawi, S., and Frangopol, D. M. (1994). "System reliability and redundancy in structural design and evaluation." *Struct. Saf.*, 16(1–2), 47–71.

Ibarra, L. F., Medina, R. A., and Krawinkler, H. (2005). "Hysteretic models that incorporate strength and stiffness deterioration." *Earthquake Eng. Struct. D*, 34(12), 1489–1511.

ICC (International Code Council). (2003). "International building code." Falls Church, VA.

LGSEA (Light Gauge Steel Engineers Association). (1998). "Lateral load resisting elements: Diaphragm design values." *Technical Note 558b-1*, Washington, DC.

Lin, S. H., Yu, W. W., and Galambos, T. V. (1988). "Fourth progress report: Load and resistance factor design of cold-formed stainless steel: Statistical analysis of material properties and development of the LRFD provisions." Dept. of Civil Engineering, Univ. of Missouri-Rolla, Rolla, MO.

Liu, P., Peterman, K. D., and Schafer, B. W. (2014). "Impact of construction details on OSB-sheathed cold-formed steel framed shear walls." *J. Constr. Steel Res.*, 101(Oct), 114–123.

Madsen, R. L., Nakata, N., and Schafer, B. W. (2011). "CFS-NEES building structural design narrative." *CFS NEES: Advancing Cold-Formed Steel Earthquake Engineering*, Baltimore.

Meimand, V. Z., and Schafer, B. W. (2014). "Impact of load combinations on structural reliability determined from testing cold-formed steel components." *Struct. Saf.*, 48(May), 25–32.

Moen, C. D. (2008). "Direct strength design of cold-formed steel members with perforations." Ph.D. dissertation, Johns Hopkins Univ., Baltimore.

Moen, C. D., and Schafer, B. W. (2009). "Elastic buckling of cold-formed steel columns and beams with holes." *Eng. Struct.*, 31(12), 2812–2824.

Moen, C. D., Tao, F., and Cole, R. (2016). "Monotonic and cyclic backbone response of single shear cold-formed steel screw-fastened connections." *Int. Colloquium on Stability and Ductility of Steel Structures*, Dept. of Steel Structures, Politehnica Univ. of Timisoara, Timisoara, Romania.

NAHB Research Center. (1999). "Innovative residential floor construction: Horizontal diaphragm values for cold formed steel framing." Upper Marlboro, MD.

Peterman, K. D. (2014). "Behavior of full-scale cold-formed steel buildings under seismic excitations." Ph.D. dissertation, Johns Hopkins Univ., Baltimore.

Peterman, K. D., and Schafer, B. W. (2013). "Hysteretic shear response of fasteners connecting sheathing to cold-formed steel studs." *CFS NEES: Advancing Cold-Formed Steel Earthquake Engineering*, Johns Hopkins Univ., Baltimore.

Peterman, K. D., Stehman, M. J. J., Madsen, R. L., Buonopane, S. G., Nakata, N., and Schafer, B. W. (2016a). "Experimental seismic response of a full-scale cold-formed steel-framed building. I: System-level response." *J. Struct. Eng.*, 10.1061/(ASCE)ST.1943-541X.0001577, 04016127.

Peterman, K. D., Stehman, M. J. J., Madsen, R. L., Buonopane, S. G., Nakata, N., and Schafer, B. W. (2016b). "Experimental seismic response of a full-scale cold-formed steel-framed building. II: Subsystem-level response." *J. Struct. Eng.*, 10.1061/(ASCE)ST.1943-541X.0001578, 04016128.

Rosowsky, B., and Ellingwood, B. R. (1991). "System reliability and load-sharing effects in light-frame wood construction." *J. Struct. Eng.*, 10.1061/(ASCE)0733-9445(1991)117:4(1096), 1096–1114.
Ross, S. M. (1995). *Stochastic processes*, Wiley, New York.
Sabelli, R., Sabol, T. A., and Easterling, W. S. (2011). "Seismic design of composite steel deck and concrete-filled diaphragms: A guide for practicing engineers." *NEHRP Seismic Design Technical Brief No. 5*, Los Angeles.
Schafer, B. W., et al. (2016). "Seismic response and engineering of cold-formed steel framed buildings." *Structures*, 8(2), 197–212.
Schafer, B. W., Li, Z., and Moen, C. D. (2010). "Computational modeling of cold-formed steel." *Thin Walled Struct.*, 48(10–11), 752–762.
SFIA (Steel Framing Industry Association). (2015). "Technical guide for cold-formed steel framing products." Falls Church, VA.
Smith, B. H., Arwade, S. R., Schafer, B. W., and Moen, C. D. (2016). "Design component and system reliability in a low-rise cold formed steel framed commercial building." *Eng. Struct.*, 127, 434–446.
Stillinger, J. R. (1955). "Lateral tests on full-scale lumber and plywood-sheathed roof diaphragms." *Symp. on Methods of Testing Building Constructions*, ASTM International, West Conshohoken, PA.
Tao, F., Cole, R., and Moen, C. D. (2016). "Monotonic and cyclic backbone response of single shear sheathing-to-cold-formed steel screw-fastened connections." *23nd Int. Specialty Conf. on Cold-Formed Steel Structures*, Baltimore.
Zhang, H., Ellingwood, B. R., and Rasmussen, K. J. R. (2014). "System reliabilities in steel structural frame design by inelastic analysis." *Eng. Struct.*, 81, 341–348.